TUTORIAL REVIEW

Hydrophobic microenvironment in catalytic C1 transformations

Siew Ping Teong, Shook Pui Chan, Xiukai Li, Jinquan Wang and Yugen Zhang*

Received 00th January 20xx,
Accepted 00th January 20xx

DOI: 10.1039/x0xx00000x

Catalytic conversion of C1 molecules, such as CO, CO_2 and CH_4, into fuels and chemicals is a pivotal area in sustainable energy technologies. This process is crucial for mitigating environmental concerns and closing the carbon cycle loop. Water is a ubiquitous by-product and plays a vital role in these transformations. The presence of water can thermodynamically shift reaction equilibria and poison catalysts, leading to decreased selectivity and efficiency. Gas permeation in multi-phase reaction systems is another challenge in efficient catalyst design. Recent advancements have shown that hydrophobic microenvironments can enhance catalytic performance in C1 transformations by water removal or enhanced gas permeation. This review explores the role of hydrophobic catalysts in key energy-related C1 transformations, focusing on syngas conversion, methane oxidation, as well as electrocatalytic and photocatalytic reduction of CO_2. By examining catalyst modifications, physical mixing with hydrophobic promoters, and other innovative catalyst designs, we highlight significant breakthroughs in improving product selectivity, yield, and catalyst longevity, emphasizing its potential to revolutionize sustainable fuel and chemical production from abundant C1 feedstocks.

1. Introduction

The catalytic conversion of C1 molecules (e.g. CO, CO_2, CH_4) into fuels and chemicals is a cornerstone of modern chemical engineering and sustainable energy technologies. C1 chemistry allows for the production of high value-added fuels and products sustainably from abundant, readily available raw materials. The three major C1 compounds of industrial significance are carbon monoxide (CO), carbon dioxide (CO_2) and methane (CH_4) which relate to several most important industrial processes including Fischer–Tropsch synthesis, methanol synthesis (CO hydrogenation), methane reforming, and emerging CO_2 to methanol process.[1-3] Water is a ubiquitous by-product and plays a vital role in these transformations.[4] The presence of water in the reaction system can thermodynamically shift the reaction equilibrium and poison the catalyst through various mechanisms, leading to side reactions, poor selectivity and low efficiency. The thermodynamic equilibrium of a reaction can be shifted toward the product side by selectively removing side products from the system.[5] Hence, great benefits are expected by removing water *in-situ* from the reaction system, such as increasing product selectivity and yield, as well as prolonging catalyst lifetime.[6-10] However, it has been impeded with challenges and much effort was devoted to solving this issue. Several strategies include using physical water absorbent,[11] water consuming chemicals,[12] water permeable membranes/channels (both inorganic and organic materials)[13-15] and creating hydrophobic microenvironment with hydrophobic polymers,[10] coatings,[8] etc. These strategies have been applied to various reactions including Fisher-Tropsch, CO hydrogenation, CO_2 to methanol, methane to methanol and also liquid (water) phase[16] reactions, including electrocatalysis[17-20] and photocatalysis,[21] demonstrating positive impacts on the reactions.

Furthermore, the hydrophobic microenvironment also leads to other functions such as gas capture and storage[17], selective mass transferring/separation[22] and improved gas-diffusion rate[23], which can also contribute to catalytic reaction efficiency, especially in multi-phase catalytic reaction systems. Over the years, various review papers on C1 catalytic transformations[24-30] and the role of water in these transformations[31] have been published. Reviews on the effect of hydrophobic catalysts on several fields have also been reported such as green chemistry[32], organic synthesis[33] and hydrophobic MOFs[34, 35]. The concept of hydrophobicity has been applied with great success on reactions such as catalytic hydrogenation[36, 37], photocatalytic reactive oxygen species (ROS) generation[16], electrocatalytic nitrogen reduction[38-42] and electrochemical O_2 reduction to H_2O_2[43, 44]. Particularly, reviews on hydrophobic catalysts for syngas conversion[45] and CO_2 reduction[46] has been published recently indicating the increasing importance of hydrophobicity in these reactions. This review will cover recent developments in hydrophobic catalyst for energy-related C1 transformations, focusing on syngas conversion, methane oxidation, as well as electrocatalytic and photocatalytic reduction of CO_2. We will

*Institute of Sustainability for Chemicals, Energy and Environment (ISCE²), Agency for Science, Technology and Research (A*STAR), 1 Pesek Road Jurong Island, Singapore 627833, Republic of Singapore. E-mail: zhang_yugen@isce2.a-star.edu.sg*

† Footnotes relating to the title and/or authors should appear here.
Supplementary Information available: [details of any supplementary information available should be included here]. See DOI: 10.1039/x0xx00000x

group these transformations into 3 major sections: 1) Thermodynamic reactions (syngas and CH_4), 2) Electrocatalytic reduction (CO_2) and 3) Photocatalytic reduction (CO_2).

2. Thermodynamic reactions

2.1. Syngas (CO/H_2) transformation

A common commercial route for converting CO to gasoline involves the use of syngas. The conversion of syngas to gasoline is a critical industrial process for upgrading coal and biomass resources. Typically, this conversion occurs through the classic Fischer-Tropsch synthesis (FTS)[47-49] or the emerging Oxide-Zeolite (OX-ZEO)[50, 51] process. During the syngas to hydrocarbons conversion, water is inevitably produced as a by-product, originating from the oxygen atom of carbon monoxide which exhibits negative effects on catalyst activity, durability, product selectivity and distributions. The carbon derivatives from the syngas conversion include CO_2 and hydrocarbons, with CO_2 being an undesired product (Scheme 1). $C_{5\text{-}12}$ hydrocarbons represent gasoline which is the desired product from this conversion. Other common hydrocarbon products may include CH_4, $C_{2\text{-}4}$ (including olefins and paraffins), $C_{8\text{-}16}$ (jet fuel) and $C_{10\text{-}20}$ (diesel). CO_2 is formed as a side product through the water-gas shift (WGS) reaction between CO and H_2O as they co-exist on the catalyst surface. The presence of water in the system will firstly promote the CO_2 formation through WGS reaction. Secondly, it will poison the catalyst and diminish the selectivity and durability of the catalyst. Ideally, removing water *in-situ* from the catalyst sites could inhibit CO_2 formation and increase the selectivity of hydrocarbons. Membrane water separation technology was typically applied to the system; however, several drawbacks limited their applications in large scale production, including (a) low water removal efficiency, (b) poor thermal and chemical stability, and (c) limited scalability and adaptability for industrial processes. These limitations are primarily due to the properties of the polymer-based water removal materials. For example, they typically demonstrate stability within the range of 200 - 300 °C, while many CO/CO_2 involved reactions require higher temperatures (300 °C and above). Recently, catalyst hydrophobization has made a breakthrough to efficiently improve catalytic performance and hydrocarbons selectivity in syngas conversion through water desorption. In this review, we will focus on the hydrophobic design of typical catalyst systems.

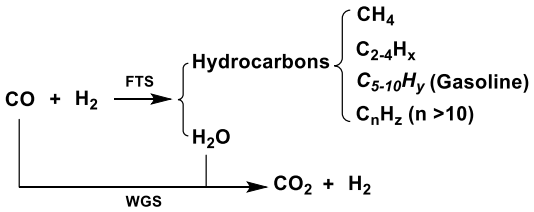

Scheme 1. Schematic diagram of syngas transformation via FTS

2.1.1. Chemical modification. Hydrophobic catalysts for syngas transformations have been reviewed recently [45] citing the importance of hydrophobic role in this area. Here, we briefly summarize a few major breakthroughs for comparison and the water diffusion behaviours in a hydrophobic catalyst system. In syngas applications, hydrophobic catalysts are typically categorized into two broad categories: 1) chemically modifying the catalyst's surface[7, 52] or 2) mixing with hydrophobic promoters[10]. Earlier efforts in 2018 were done through silylation[53] and methylation[54] to modify catalyst's hydrophobicity and improve FTS selectivity but with limited success (Table 1, Entry 1-2).

As the example of chemically modified catalysts for FTS, a core shell FeMn@Si hydrophobic catalyst[7] was developed by Xu et al. through a modified Stöber method with nanorod Fe_2O_3. The homogenous SiO_2 shell encapsulated the Fe_2O_3 (Fe@Si), where hydrophobic $-CH_3$ group was then introduced onto the surface through silanization reaction (Fe@Si-c) (Figure 1a) followed by deposition of Mn (FeMn@Si-c). FTIR and XRD analysis showed that during the syngas transformation, iron oxides disappeared and completely converted to iron carbides in the spent Fe@Si-c, while both iron oxides and iron carbides were detected in the spent Fe@Si, suggesting that the hydrophobic shell effectively tune the iron phases during the reaction. It demonstrated that the hydrophobic surface on Fe@Si-c could effectively facilitate rapid water desorption and restrict its entry into the catalyst, thus inhibited the conversion of iron carbides back to iron oxides. Hence, the CO_2 selectivity was obviously reduced (Figure 1b) with increased olefin selectivity. The resulting catalyst hindered the WGS side reaction and protected against catalyst poisoning with a low CO_2 selectivity of 13 % and high total olefins selectivity of 75 % at 56.1 % CO conversion (Table 1, Entry 3). The selectivity of undesired C1 by-products and the olefin selectivity in total products remained relatively stable during the 100 h stability test.

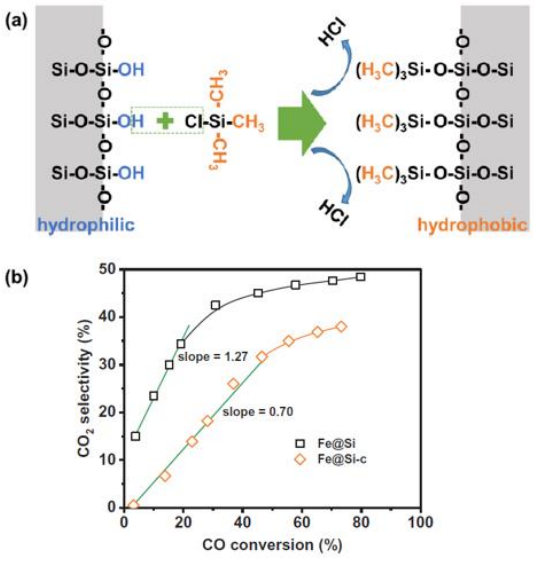

Figure 1. a) Hydrophobic $-CH_3$ group surface modification via silanization reaction using chlorotrimethylsilane (TMCS) and b) CO_2 selectivity–CO conversion curve, hydrophobic Fe@Si-C catalyst demonstrated much lower CO_2 selectivity at same CO conversions. Reproduced from ref. [7] with permission from AAAS, copyright 2021.

Table 1. Comparison of various hydrophobic catalysts and their activities on syngas transformation.

Entry	Catalyst	CO conversion (%)	Selectivity (%)		Contact angle (◦)	Ref
			Products	CO_2		
1	tMo-Me modified CoRe/γ-Al_2O_3	50.0	8.7[a] (CH_4) 8.4[a] (C_{2-4}) 82.9[a] (C_5^+)	n.d.	n.d.	53
2[b]	CH_3-modified Fe_2O_3@SiO_2	50.0	37 (CH_4) 55 (C_{2-4}) 5 (C_5^+)	<5	126.9	54
3[c]	FeMn@Si	56.1	10.0 (CH_4) 65.0 (total olefins)	13.0	137.6	7
4[c]	FeNa@Si-c	49.8	62.5 (C_{5-11})	14.3	117.0	52
5[b]	CoMnC/PDVB	63.5	4.8 (CH_4) 71.4 (C_{2-4}) 16.9 (C_5^+)	46.3	145.0	10

[a]CO_2 free selectivities; [b] 120 h stability test; [c] 100 h stability test; n.d. not determined

Later, the group probed into the water diffusion behaviours through designing a bifunctional hydrophobic FeNa@Si-c catalyst by introducing non-polar –CH_3 group on the catalyst support, combined with nanosized HZSM-5 zeolite to obtain a high selectivity for gasoline of 62.5 %, low CO_2 selectivity of 14.3 % at 49.8 % CO conversion[52] (Table 1, Entry 4). In contrast, the Fe-based catalyst before methylation or after removal of –CH_3 group showed a high CO_2 selectivity, suggesting the hydrophobicity of the catalyst was crucial to inhibit CO_2 formation. Molecular dynamics simulations showed the diffusion model of the water molecules through hydrophilic surface (Figure 2a) was bidirectional while the diffusion through hydrophobic catalyst was unidirectional (Figure 2b). While water diffusion through hydrophobic B1 surface was not observed, they can still leave from the pore surface. Hence, water produced during syngas conversion was unable to diffuse into the hydrophobic catalyst, hindering re-adsorption and this is crucial in reducing the unwanted WGS side reaction.

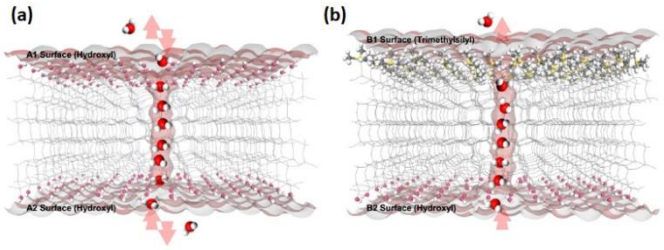

Figure 2. Diffusion model of water molecules through (a) structure A, bidirectional diffusion and (b) structure B, one-way diffusion. Reproduced from ref. [52] with permission from John Wiley and Sons, copyright 2023.

2.1.2. Physical mixing. Unlike the chemical modification route for hydrophobic catalyst, Fang et al. took a simple approach by physically mixing a hydrophobic promoter, poly(divinylbenzene) (PDVB) with cobalt-manganese carbide (CoMnC) catalyst[10]. The hydrophobic promoter was randomly distributed in the catalyst granules. The resulting CoMnC/PDVB catalyst improved CO conversion from 32.2 % to 63.5 % and increased light olefins (C_{2-4}) selectivity from 60.8 % to 71.4 % (Table 1, Entry 5). However, CO_2 selectivity is relatively stable at around 46.3 % to 48.1 %. The catalyst performance was relatively stable up to at least 120 h.

While the chemical modification route dramatically reduces CO_2 formation and enhances olefins selectivity, the CO conversion has been hovering around 50 %. On the other hand, the mixing approach is simple and could be useful in terms of upscaling industrial processes. However, while it boosted CO conversion, the CO_2 selectivity remained relatively high. It is noteworthy that hydrophobic systems have also been applied on CO electroreduction[55] or photothermal conversion of syngas/CO[56, 57], albeit with low CO conversion. Further research can be done to obtain a balanced and optimized approach for efficient syngas conversion.

2.2. CH_4 transformation

CH_4 is a key molecule for converting into fuels and high-value chemicals like olefins and aromatics, which are essential for commodities such as cosmetics, lubricants, detergents, and polymers[58]. CH_4 catalytic conversion to value-added products is one of the most challenging tasks in C1 chemistry due to methane's high C-H bond strength (104 kcal/mol) and stability. Hence, these chemicals are usually produced from CH_4 through multi-step processes via syngas. In dry reforming of methane (DRM), which converts CH_4 and CO_2 into syngas, water indirectly affects the process through side reactions and causes catalyst deactivation due to coking. Here, hydrophobic catalyst design is able to achieve high catalytic activity and stability[59] with high CO_2 and CH_4 conversions of 70 % and 68 % at 700 °C.

However, the direct conversion of methane to valuable fuels remains attractive due to its potential in contributing to a green and sustainable environment. Water plays a crucial role

in both gas-phase and liquid-phase methane transformations. Li et al. studied the effect of water on long-term catalyst stability and its inhibition mechanisms on palladium-based catalysts[60], which are highly active for methane oxidation[61-63]. They found that hydroxyls from water block active sites on palladium, hindering oxygen adsorption and reducing catalyst efficiency. This prevented oxygen vacancies from being filled, contributing to water's inhibitory effect on methane combustion[60]. Thus, controlling water presence through removal techniques or hydrophobic catalysts can improve the efficiency, selectivity, and longevity of these catalytic conversion reactions.

2.2.1. Chemical modification/coating. In methane oxidation, Wang et al. prepared hydrophobic dB-ZSM-5, treated with tetrapropylammonium bromide and supported on Rh single-atom catalysts, which showed superior performance for methane partial oxidation compared to hydrophilic Rh catalysts on ZSM-5[64]. The catalysts were prepared by deboronation of B-ZSM-5 with HCl, treatment with H_3RhCl_6, and calcination, resulting in isolated Rh on hydrophobic dB-ZSM-5. The hydrophobic micropores of dB-ZSM-5 could absorb hydrophobic CH_4 under low pressure, facilitating the catalytic reaction. The hydrophobic dB-ZSM-5 supported Rh catalysts were more active for methane conversion into C1 and C2 oxygenates under low pressure conditions (0.3 MPa CH_4, 0.1 MPa CO and 0.05 MPa O_2). These catalysts exhibited higher activity and better selectivity for C1 oxygenates compared to hydrophilic Rh on ZSM-5, which was more selective for CH_3COOH.

Focusing on the impact of hydrophobic microenvironments on methane selective oxidation, Li et al. enhanced the water resistance of MOF-catalysts by coating them with hydrophobic polydimethylsiloxane (PDMS)[65]. This catalyst created coordinatively unsaturated Cu(I) sites that facilitated H_2O_2 dissociation into •OH, forming Cu(II)-O active sites for methane C–H bond activation. The PDMS coating process was treated at 200 °C and 235 °C to give Cu-BTC-P200 and Cu-BTC-P235 catalysts. Cu-BTC-P235 catalyst treated at 235 °C has a much strong PDMS coating and achieved higher productivity of 10.67 mmol $gcat.^{-1}$ h^{-1} and high selectivity of 99.6% for C1 oxygenates, particularly CH_3OH and CH_3OOH, Figure 3[65]. Additionally, the team developed surface hydrophobic CUS-M-P-210 catalyst with unsaturated Fe(II) sites by similar PDMS modification process, achieving a record yield of 83.13 mmol $gcat.^{-1}$ h^{-1} with selectivity of approximately 100% for C1 oxygenates[66]. Both approaches demonstrated efficient oxidation of methane and good catalyst durability by using hydrophobic MOF-based heterogenous catalysts.

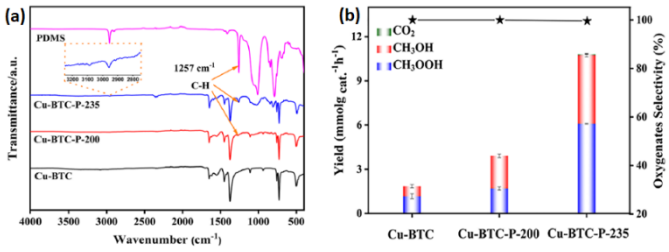

Figure 3. a) FTIR spectra of PDMS, pristine, and coated Cu-BTC. Cu-BTC-P-235 exhibited a clear and strong PDMS signal. b) The yield and selectivity of oxygenates from Cu-BTC, Cu-BTC-P-200, and Cu-BTC-P-235 in the oxidation of methane with 50 °C, 3 MPa CH_4, and 10 mL H_2O_2 aqueous solution (0.25 M). Compared with Cu-BTC-P-200, Cu-BTC-P-235 showed higher catalytic activity, better hydrophobic effect and more stable structure in the liquid-phase reaction system different reaction conditions[65].

Following the same direction, Hwang et al. reported a method to control the surface hydrophobicity of zeolite catalysts via simple carbon coating, enhancing their performance in aqueous-phase selective methane oxidation with H_2O_2[67]. By adjusting the amount of furfuryl alcohol (FA) and hydrophobicity on surface of parent materials H-ZSM-5 and Fe-ZSM-5, the catalytic performance increased with carbon content up to a point, then decreased with further carbon addition. The product yield per H_2O_2 consumed followed a similar trend to that of carbon content, as did the catalytic performance. The improved performance was evident when the carbon content was not high enough to block the pores, highlighting surface hydrophobicity as a crucial factor in catalytic activity. Other catalysts with controlled surface hydrophobicity have shown high activity in similar reactions. For example, AuPd alloy nanoparticles encapsulated within organosilane-modified zeolites showed high catalytic activity with in situ-generated H_2O_2 from H_2 and O_2[8]. The hydrophobic silane trapped H_2O_2 inside the catalyst, maintaining a high local concentration and improving productivity.

2.2.2. Biomimetic catalyst. Inspired by natural enzymes methane monooxygenases (MMOs), Sui et al. developed a biomimetic catalyst for methane oxidation by incorporating Fe-porphyrin into the MOF UiO-66 and furnished with hydrophobic saturated monocarboxylic fatty acids[68]. The resulting catalyst Fe^{3+}@UiO-66-Cn demonstrated high efficiency for converting CH_4 to methanol at 50°C, and its selectivity to CH_3OH is enhanced by hydrophobic modifications that adjust the Fe active sites' electronic state, improving CH_4 adsorption while limiting amount of H_2O_2 at Fe sites.

3. Electrocatalytic reduction reactions

In CO_2 conversion, catalytic hydrogenation of CO_2 to hydrocarbons, mainly through syngas (CO) or methanol as intermediates, is the most common approach[69] and hydrophobicity can also facilitate its reaction[70-74]. Recently, electrocatalytic reduction of CO_2 has emerged as a sustainable route towards generating valuable hydrocarbon fuels and value-added chemical feedstocks using renewable energy technologies, representing one of the most promising approaches in CO_2 utilization[75]. However, in the multi-phase electrocatalytic system, CO_2 has low solubility and diffusion coefficient in aqueous media (33 mM at 1 atm and 25 °C), leading to poor transport and mass transfer of CO_2 to the catalyst surface[76]. Besides, the redox potentials for CO_2 reductions to various desired products are similar to that for hydrogen evolution which led to competitive hydrogen evolution reaction (HER) and reduced Faradaic efficiency (FE) (Figure 4)[17, 77].

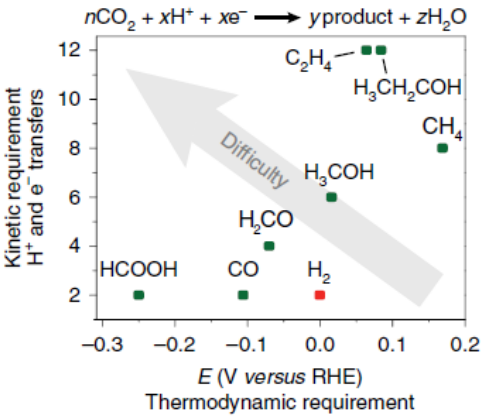

Figure 4. Kinetic versus thermodynamic requirement of various CO_2 electroreduction reactions. Reproduced from ref. [17] with permission from Springer Nature, copyright 2019.

Gas diffusion electrodes (GDEs), which have porous structures containing a gas diffusion layer and catalyst layer may help to enhance gas transport rates[78]. However, it is insufficient to suppress HER. Various strategies were proposed to improve catalyst surface gas transportation, such as nano-sized catalytic surface areas[79-82], Cu-loaded carbon supports[83-85], surface oxides[86-88] etc. Recently, hydrophobicity has emerged as a significant contributing factor for improving CO_2 reduction selectivity by limiting water accessibility and increasing CO_2 concentration near electrode surface / catalytic sites[46, 89]. We briefly summarized some hydrophobic electrocatalysts in the section below.

3.1. Surface coating / deposition

Wakerley et al. pioneered the study on the effect of hydrophobicity on Cu surface to improve selective CO_2 reduction[17]. The group developed a superhydrophobic surface through modification of hierarchically structured Cu dendrites by coating with a monolayer of 1-octadecanethiol (Figure 5). Contact angle measurements increased from 17° to a) 153° after hydrophobic treatment and b) 143° after 12 hours of electrolysis, indicating the hydrophobic surface was durable. When CO_2 gas stream was introduced from the bottom of the cell, CO_2 was visibly trapped at the electrolyte-electrode interface, causing a bubble to engulf the entire electrode surface. This gas-filled void resulted in high CO_2 concentration at the Cu surface and led to drastic decreased in H_2 production (from 71 % to 10 % FE) with increased CO_2 reduction (from 24 % to 86 %), yielding C_{1-2} products: CO (3 %), methane (7 %), ethylene (56 %), ethanol (17 %) and acetic acid (1 %) (Table 2, Entry 1). However, reduced current density occurred since the Cu active sites are largely blocked by the hydrophobic coating.

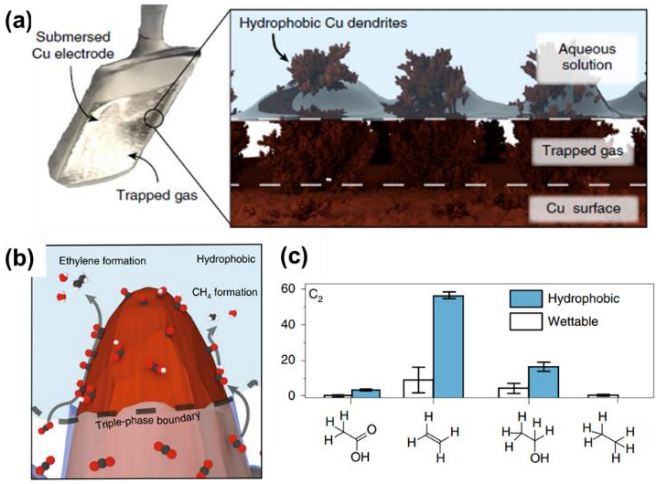

Figure 5. (a) Hydrophobic dendritic Cu surface gas-trapping between the solution-solid interfaces for aqueous CO_2 reduction, (b) Mass transport from the triple-phase boundary between the electrolyte, electrode and gaseous CO_2 with the key products formed on the surface. (c) Product formation FEs at the hydrophobic versus wettable dendrite. Reproduced from ref. [17] with permission from Springer Nature, copyright 2019.

Nevertheless, many research studies benefited from this concept and much work have since been done to study the hydrophobic effect on electrocatalytic reduction of CO_2 on various metal catalytic systems, by using alkanethiols[90-93], fluorosilane (FAS)[94], polytetrafluoroethylene (PTFE) or other fluorinated polymer additives[95-101]. Interestingly, Niu et al. achieved superhydrophobicity with a contact angle of 154° through electrodeposition, inspired by the hierarchical structure of Setaria leaves, without using any hydrophobic coatings[102]. More selected examples are summarized in Table 2.

Xing et al. used chemically inert polytetrafluoroethylene (PTFE) as the hydrophobic component in a gas-diffusion electrode (GDE) cell. [18] In a GDE cell, one side of the catalyst was exposed to CO_2 gas, which diffused through the pores of carbon fibre paper (CFP) and passed through the microporous layer (MPL) to reach the catalyst (Figure 6a). This cell configuration may solve the mass transport issues but since the catalyst are often wetted by electrolyte, the reaction still proceeds via dissolved CO_2 and the competing HER remains a problem. Here, the PTFE-added Cu electrode is hydrophobic and not wetted by electrolyte (Figure 6b). This reduces the diffusion layer thickness, accelerates CO_2 mass transport, and increases CO_2 concentration. CO_2 reduction (C_{1-2} products) increased from a range of 35 – 50 % FE (without PTFE) to 68 – 76 % FE (with PTFE) and H_2 production decreased from a range of ~44 – 61 % FE (without PTFE) to 5 – 26 % FE (with PTFE) at various flow rates. Contact angle of the bare Cu/C electrode dropped from 144.2° to 55.4° while contact angle of Cu/C/PTFE electrodes ranged from 150.8° to 144.7° after 2 h of electrolysis (Table 2, Entry 2). The slight difference suggested that the PTFE particles can preserve the hydrophobicity and prevent catalyst from flooding. A high partial current density of ~250 mA/cm^2 was reached at -1.0 V. In another modified Cu/PTFE electrode example, various quaternary ammonium

group-functionalized polynorborene ionomers were used[103] to modify Cu/PTFE electrode with a water contact angle of 137°, high C_{2+} FE of 90 % and low H_2 production of ~9 % (Table 2, Entry 3).

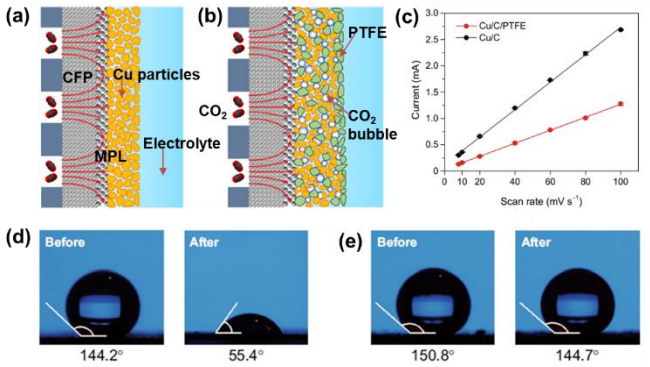

Figure 6. Schematic diagram of a) solid-liquid interface in a regular GDE cell (Cu/C) and b) solid-liquid-gas interface in a GDE cell with PTFE nanoparticles inside catalyst layer which can hold CO_2 bubbles (Cu/C/PTFE). (c) Double-layer charging current plotted against the CV scan rate for the two electrodes. Contact angle measurements of d) bare Cu/C electrode and e) Cu/C/PTFE electrodes after 2 h of electrolysis.[18]

In another report for electroreduction of CO_2 to HCOOH, Cu/Sn nanowires were modified with trimethoxy (1H, 1H, 2H, 2H-heptadecafluorodecyl)-silane (FAS) and demonstrates high FE_{HCOOH} of 94.17 % compared to 76.44% with that of the hydrophilic electrode, maintaining its activity (FE_{HCOOH} 91.36 %) after 7 h of reaction (Table 2, Entry 4).[104] Bismuth (Bi) nanospheres were loaded on porous carbon nanosheets (Bi-C) to form a superhydrophobic electrode for efficient production of formate with high FE of 97.4% (Table 2, Entry 5).[105] More Bi-catalyzed hydrophobic CO_2 reduction to formate is summarized in Table 2, Entries 6-7.[106, 107] Hydrophobic electrocatalytic system has also been demonstrated in CO_2 to CO reaction (Table 2, Entries 8 – 10)[108-110]. A hydrophobic Ag nanocatalyst were prepared *in situ* in cyclohexene to give a stable FE_{CO} of 70 % for 8 h.[108] Hydrophobic zinc foam deposited with zinc myristate (Zn $[CH_3(CH_2)_{12}COO]_2$) can also improve FE_{CO} from 81.87% to 91.8% at -1.9 V for 10 h.[109]

3.2. Electrospinning and annealing

Using a H-cell configuration, Li et al. integrated carbon nanotubes (CNT), core–shell CuO nanospheres and PTFE into wire membrane to overcome low current density. This interesting design led to a multifunctional superhydrophobic, conductive and hierarchical wire membrane denoted as CuO/F/C(w) with a high water contact angle of 151.2° (Table 2, Entry 11).[111] This design increases the exposure of CuO and maximises the contact of CuO nanospheres and CO_2 with good conductivity, leading to improved selectivity of CO_2 reduction (64.9 – 73.6 % FE) compared to bare CuO (14.5 – 33.9 % FE) for C_{1-3} products and reduced H_2 production (25.6 – 36.0 % FE) compared to bare CuO (64.0 - 84.9 % FE) under various potential ranging from -1.0 V to -1.5 V. However, contact angle dropped slightly to 129.6° after 10 h of electrolysis, indicating possibly slight flooding of the electrode. In industrial practice, it is desirable to achieve a current density >200 mA cm^{-2} with stability of >80,000 h and product selectivity over 90%.[112] While product selectivity has been largely improved, stability tests and general low current density is still a work-in-progress.

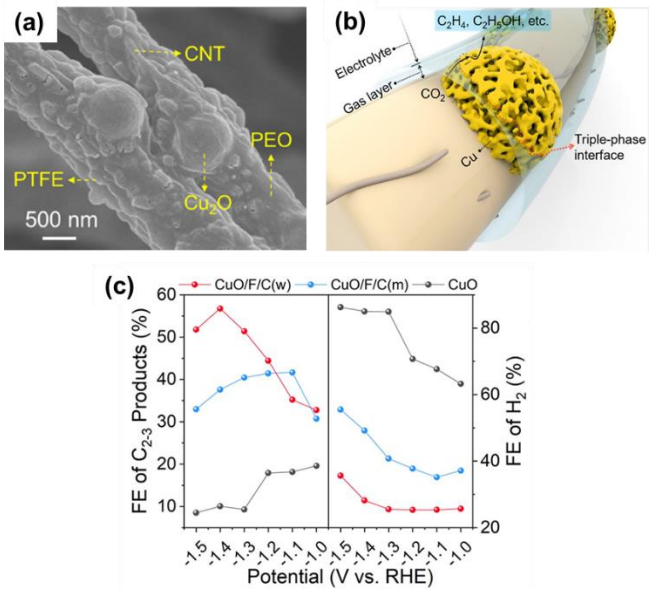

Figure 7. (a) FESEM images of the PEO/Cu_2O/F/C(w) membrane. (b) Schematic diagram of the role of triple-phase interfaces in CO_2 electroreduction. (c) Comparison of FE of C_{2-3} products and H_2 at various potentials. Hydrophobic catalyst has much higher C_{2-3} product selectivity. Reproduced from ref. [111] with permission from John Wiley and Sons, copyright 2023.

4. Photocatalytic reduction reactions

Sunlight-driven photocatalytic CO_2 reduction is gaining attention as a promising renewable solution to the current environmental problems.[113-116] Both homogenous[117-120] and heterogenous[121-125] transition metal catalysts have been explored in the photoreduction of CO_2. Similar to electrocatalytic system, the competing HER is one of the main issues that hinders high efficiency and unfavourable for commercial utilization. Herein, hydrophobicity also demonstrated potential to improve the selectivity in photocatalytic CO_2 reduction.

Table 2. Comparison of various hydrophobic electrocatalysts and their activities.

Entry	Catalyst	Faradaic efficiency (% FE)		Contact angle (◦)[a]	Condition	Ref
		Products	H_2			
1	Cu/octadecanethiol	86 (C_{1-2})	10	153 / 143[b]	0.1 M $CsHCO_3$ -30 mA/cm^2 -1.6 V	17
2	Cu/C/PTFE	68 - 76 (C_{1-2})	5 - 26	150.8 / 144.7[c]	1 M KOH ~250 mA/cm^2 -1.0 V	18
3	D18-Cu $KHCO_3$	90 (C_{2+})[e]	~9	137 / n.d.	0.1 M $KHCO_3$ 223 mA/cm^2 -4.2 V	103
4	HB-Cu NW/Sn	94.17 (HCOOH)	3.81	152.0 / 140.7[f]	0.1 M $KHCO_3$ 17.83 mA/cm^2 -1.2 V	104
5	Bi-C/723	97.4 ($HCOO^-$)	n.d.	153 / n.d.	0.5 M $KHCO_3$ 100 mA/cm^2 -1.06 V	105
6	Bi_2O_3@PTFE-NC	>90 ($HCOO^-$)	~7	120.1 / n.d.	0.5 M $KHCO_3$ -100 mA/cm^2 -1.37 V	106
7	Bi_2O_3@C/HB	>93 ($HCOO^-$)	<5	134.8 / n.d.	0.5 M $KHCO_3$ 102 mA/cm^2 -1.7 V	107
8	AgNano-Pre-100	70 (CO)[g]	n.d.	n.d.	0.1 M $KHCO_3$ 11-18 mA/cm^2 -1.2 V	108
9	HPB/Zn-1	91.8 (CO)[d]	~10	136 / n.d.	0.1 M $KHCO_3$ -5.16 mA/cm^2 -1.9 V	109
10	PTFE-H-NiNCNTs-CNF	95.6 (CO)	~5	n.d.	0.5 M $KHCO_3$ 4.56 mA/cm^2 -1.4 V	110
11	CuO/F/C(w)	73.6 (C_{1-3})	28.2	151.2 / 129.6[d]	0.5 M $KHCO_3$ 68.9 mA/cm^2 -1.4 V	111

[a]contact angle after hydrophobic treatment / after stability test; [b]12 h of electrolysis; [c]2 h of electrolysis; [d]10 h of electrolysis; [e]55 h of electrolysis; [f]7 h of electrolysis; [g]8 h of electrolysis; n.d. not determined

4.1. Chemical modification / surface coating

In the photocatalytic reduction of CO_2, HER is also a major competing reaction and largely hinders the selectivity of carbon products. Hydrophobic photocatalysts, as a potential solution for high selectivity of carbon products, are largely synthesized through chemical modification with long alkyl chains. Li et al. found that the hydrophobic photocatalyst grafted with 1H, 1H, 2H, 2H-perfluorodecanethiol effectively improved the CO_2 adhesion, resulting in fast CO_2 mass transfer with hydrophobic polymeric carbon nitride nanosheet loaded with Pt particles (Pt/*o*-PCN)[22] (Table 3, Entry 1). Selectivity of CO_2 reduction improved from 5.3 % to 84.2 % with negligible H_2 formation. In a different trial to increase absorption of CO_2 on the catalyst surface, ultrathin Bi_2WO_6 nanosheets were prepared, together with a hydrophobic surface using hexadecyl trimethyl ammonium bromide (CTAB). This enhanced the CO_2 concentration on the surface, and improved CO production rate dramatically from 0.40 to 7.12 μmol g^{-1} h^{-1}, which is around 18 times higher than the hydrophilic version. CH_4 formation was also detected at a rate of 0.63 μmol g^{-1} h^{-1}, which was previously not detected (Table 3, Entry 2).[126] Other chemical modification efforts for applying hydrophobic effect in gas-phase photocatalytic system included a graphitic carbon nitride (g-C_3N_4) photocatalyst grafted by CF_2 groups (CF_2-TCN)[127] and a PTFE coated Cu_2O/Sn/PTFE photocathode[128], and improved catalytic efficiency and selectivity were achieved (Table 3, Entries 3-4).

4.2. Physical treatment

In addition to chemical modification of catalyst surface, physical treatment or fabrication could also change catalyst properties/environment, such as crystallinity, surface roughness and morphology, could also alter the hydrophobicity of catalyst, therefore collectively improving catalyst performance. A nanoparticulate CoP-600 cocatalyst was developed under thermal treatment with improved crystallinity and hydrophobicity.[129] While the contact angle only increases from 10.8° (pristine CoP) to 41.8°, CO production rate shows 3.4 times increase from 20 μmol/h ($CO_{sel.}$ 28.4 %) to 68.1 μmol/h ($CO_{sel.}$ 67 %) and H_2 generation decreased from 50 μmol/h to 30 μmol/h in the hydrophobic system (Table 3, Entry 5). CO and H_2 evolution rate also remained relatively stable during six successive runs. Interestingly, an amphiphilic CoOx/biochar (CDB) with a synergistic effect on improved carrier separation and migration efficiency was also developed to faciliate photocatalytic reduction of CO_2 under water/organic system (Table 3, Entry 6).[130] Another hydrophobic photocatalyst with TiO_2 nanosheet arrays was grown on porous hydrophobic carbon paper Ni@N-doped TiO_2-HCP to mitigate HER and improve photocatalytic reduction of CO_2 to CH_4 with a selectivity of 74.6% (Table 3, Entry 7).[131]

4.3. Biomimetic catalyst

In natural photosynthesis, hydrophobic lipid membranes play important roles[132, 133]. To mimic this, Yang et al. used metallogels (LG/Nico-Co) based on the co-assembly of lipid-like molecules, L-glutamic acid lipid derivatives (such as LG/Nico) and Co ions to achieve efficient photocatalytic reduction of CO_2 to CO.[21] Indeed, the highest CO production of ~2.09 x 10^5 μmol g^{-1} with CO/H_2 selectivity of 90 % was presented within 24 h of photocatalysis and catalytic stability maintained for at least three consecutive runs (Table 3, Entry 8). The co-assembly formed bilayer nanostructures with tightly packed alkyl chains and localized active sites, giving rise to a hydrophobic microenvironment for catalysing the CO_2 reduction reaction (Figure 8). Both the hydrophobic environment and Co active sites configuration contribute to achieve synergistic effects during the photocatalytic reaction.

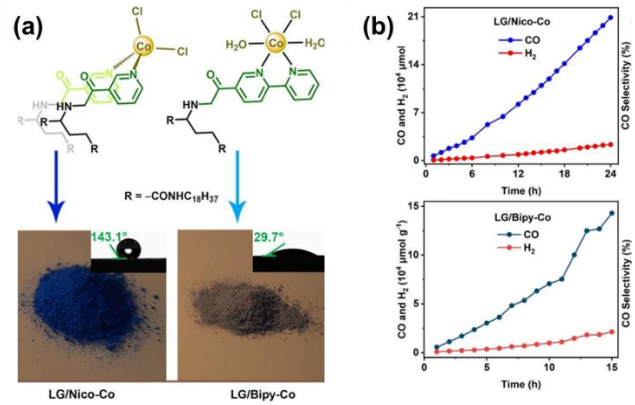

Figure 8. (a) Different complexes between Co ions and LG/Nico or LG/Bipy; insets: the contact angles of the LG/Nico-Co xerogel and LG/Bipy-Co xerogel. (b) Time-dependent CO and H_2 evolution upon visible-light irradiation for LG/Nico-Co and LG/Bipy-Co photocatalytic system. Reproduced from ref. [21] with permission from John Wiley and Sons, copyright 2022

Table 3. Comparison of various hydrophobic photocatalysts and their activities.

Entry	Photocatalyst	Activity (μmol/h)	Selectivity (%)	H_2 (μmol/h)	Contact angle (◦)[a]	Ref
1	Pt/*o*-PCN	2.86 (CO) 1.36 (CH_4)	87.9	Negligible	120 / n.d.	22
2	BWO-C2	7.12 (CO)[b] 0.63 (CH_4)[b]	n.d.	Negligible	125 / 122[c]	126
3	CF_2-TCN modified g-C_3N_4	30.9 (CO)[b] 7.39 (CH_4)[b]	54 (CO) 46 (CH_4)	n.d.	80 / n.d.	127
4	Cu_2O/Sn/PTFE	FE_{CO} 95.1 %	n.d.	FE_{H2} 3.8 %	129.5 / n.d.	128
5	CoP-600	68.1 (CO)	67	30	41.8 / n.d.	129
6	CDB-3	48.3 (CO)	71	19.7	37 / n.d.	130
7	Ni@N-doped TiO_2-HCP	139.02 (CO)[d] 134.17 (CH_4)[d]	74.6 (CH_4)	48.96[d]	n.d.	131
8	LG/Nico-Co	8697 (CO)[b]	90	~1000[b]	143.1 / n.d.	21

[a]contact angle after hydrophobic treatment / after stability test; [b]reported in μmol $g^{-1}h^{-1}$; [c]4 runs for 20 h; [d]reported in μmol $m^{-2}h^{-1}$; n.d. not determined

The emerging electrochemical and photocatalytic reduction of CO_2 are undoubtedly promising avenues to replace fossil fuel based-production processes and represent a potential step towards carbon capture and utilization. However, the relative low efficiencies have hindered commercial adoption. The concept of hydrophobicity to increase gas concentration near the catalyst surface has nonetheless made a huge breakthrough in solving the issues due to low CO_2 solubility, poor CO_2 diffusion and reduces the competing HER. Overall, integrating hydrophobicity into electrochemical and photocatalytic CO_2 reduction systems shows great promise in advancing these technologies towards practical application, offering sustainable alternatives to traditional fossil fuel-dependent processes.

5. Conclusion and future perspectives

The historical significance of C1 chemistry has regained importance due to its potential in closing the carbon cycle loop to produce high value-added fuels and products in a sustainable way from the abundant, readily available C1 components such as CO, CO_2 and CH_4. Water is recognized as the root cause to the issues contributing to poor efficiency and hinders potential large-scale applications. The implementation of hydrophobic microenvironments represents a transformative approach to enhance performance in catalytic C1 transformations by effectively managing water removal and enhancing gas permeation. These microenvironments can be created using hydrophobic materials such as silanes, fluorinated compounds, certain polymers and other innovative designs. Primary mechanisms include 1) phase separation of water to reduce water accessibility and contact with catalyst, thus minimize inhibitory effects; 2) water adsorption and desorption to enable efficient water removal and 3) microenvironmental hydrophobicity to prevent water accumulation, thus increasing gas concentration and maintaining high catalytic activity and stability. These advancements underscore the importance of hydrophobicity and its potential to drive sustainable and efficient fuel and chemical production. By repelling water and concentrating CO_2 near the catalyst surface, hydrophobic catalysts can offer significant advantages for electrocatalytic and photocatalytic C1 transformations by enhancing efficiency, selectivity and stability.

Although the mechanism of hydrophobicity preventing catalyst deactivation in C1 transformation is more specific and highly dependent on individual reactions, the water-phobic and gas-philic mechanism are rather general and can be applied into all related catalytic systems. The hydrophobic catalytic system could be applied into more important transformations which deal with water and/or gases, for example thermo-catalytic CO_2 to methanol reaction [70-72] and even biomass to chemical transformations.

While the incorporation of hydrophobic microenvironments has shown promising results with the selectivity and production rate largely boosted, challenges remain in 1) stability/durability of catalyst hydrophobicity; 2) scalability for industrial applications and 3) detailed mechanistic understanding. Future research should focus on exploring more important reaction systems and designing durable hydrophobic catalytic materials, optimizing hydrophobic microenvironmental designs, and integrating these systems into large scale processes. Detailed mechanisms can be investigated by using advanced characterization techniques and computational modelling to gain deeper insights into the interactions between water molecules and hydrophobic surfaces, guiding the development for more effective catalytic systems. By addressing these challenges and leveraging the benefits of hydrophobic microenvironments, continued innovation and future research can significantly advance the field of catalytic C1 transformations, contributing to a more sustainable and efficient chemical process.

Conflicts of interest

There are no conflicts to declare.

Acknowledgements

This work was supported by the Institute of Sustainability for Chemicals, Energy and Environment (ISCE^2), Agency for Science, Technology and Research (A*STAR), Singapore, and the National Research Foundation, Prime Minister's Office, Singapore under its Campus for Research Excellence and Technological Enterprise (CREATE) programme (Development of advanced catalysts for electrochemical carbon abatement).

Notes and references

1. J. Bierhals, in *Ullmann's Encyclopedia of Industrial Chemistry*, 2001, DOI: https://doi.org/10.1002/14356007.a05_203.
2. Inventory of U.S. Greenhouse Gas Emissions and Sinks | US EPA, https://www.epa.gov/ghgemissions/inventory-us-greenhouse-gas-emissions-and-sinks, (accessed July 16, 2024).
3. M. Bachmann, S. Völker, J. Kleinekorte and A. Bardow, *ACS Sustainable Chem. Eng.*, 2023, **11**, 5356-5366.
4. T. N. Do, C. You and J. Kim, *Energy Environ. Sci.*, 2022, **15**, 169-184.
5. I. S. Metcalfe, B. Ray, C. Dejoie, W. Hu, C. de Leeuwe, C. Dueso, F. R. García-García, C.-M. Mak, E. I. Papaioannou, C. R. Thompson and J. S. O. Evans, *Nat. Chem.*, 2019, **11**, 638-643.
6. M.-H. Hyeon, H.-G. Park, J. Lee, C.-I. Kong, E.-Y. Kim, J. H. Kim, S.-Y. Moon and S. K. Kim, *Nat. Commun.*, 2023, **14**, 1673.
7. Y. Xu, X. Li, J. Gao, J. Wang, G. Ma, X. Wen, Y. Yang, Y. Li and M. Ding, *Science*, 2021, **371**, 610-613.
8. Z. Jin, L. Wang, E. Zuidema, K. Mondal, M. Zhang, J. Zhang, C. Wang, X. Meng, H. Yang, C. Mesters and F.-S. Xiao, *Science*, 2020, **367**, 193-197.
9. H. Li, C. Qiu, S. Ren, Q. Dong, S. Zhang, F. Zhou, X. Liang, J. Wang, S. Li and M. Yu, *Science*, 2020, **367**, 667-671.
10. W. Fang, C. Wang, Z. Liu, L. Wang, L. Liu, H. Li, S. Xu, A. Zheng, X. Qin, L. Liu and F.-S. Xiao, *Science*, 2022, **377**, 406-410.
11. W. Huang, X. Zhang, A.-C. Yang, E. D. Goodman, K.-C. Kao and M. Cargnello, *ACS Catal.*, 2020, **10**, 8157-8167.
12. H. Ohno, M. Ikhlayel, M. Tamura, K. Nakao, K. Suzuki, K. Morita, Y. Kato, K. Tomishige and Y. Fukushima, *Green Chem.*, 2021, **23**, 457-469.
13. S. Dzuryk and E. Rezaei, *Ind. Eng. Chem. Res.*, 2020, **59**, 18907-18920.
14. N. Diban, A. T. Aguayo, J. Bilbao, A. Urtiaga and I. Ortiz, *Ind. Eng. Chem. Res.*, 2013, **52**, 10342-10354.
15. Y. Ban, N. Cao and W. Yang, *Research*, 2020, **2020**, 1583451.
16. H. Zhou, X. Sheng, Z. Ding, X. Chen, X. Zhang, X. Feng and L. Jiang, *ACS Catal.*, 2022, **12**, 13690-13696.
17. D. Wakerley, S. Lamaison, F. Ozanam, N. Menguy, D. Mercier, P. Marcus, M. Fontecave and V. Mougel, *Nat. Mater.*, 2019, **18**, 1222-1227.
18. Z. Xing, L. Hu, D. S. Ripatti, X. Hu and X. Feng, *Nat. Commun.*, 2021, **12**, 136.
19. Z. Fan, H. Zhao, K. Wang, W. Ran, J.-F. Sun, J. Liu and R. Liu, *Environ. Sci. Technol.*, 2023, **57**, 1499-1509.
20. X. Yang, H. Ding, S. Li, S. Zheng, J.-F. Li and F. Pan, *J. Am. Chem. Soc.*, 2024, **146**, 5532-5542.
21. G. Yang, S. Li, N. Li, P. Zhang, C. Su, L. Gong, B. Chen, C. Qu, D. Qi, T. Wang and J. Jiang, *Angew. Chem. Int. Ed.*, 2022, **61**, e202205585.
22. A. Li, Q. Cao, G. Zhou, B. V. K. J. Schmidt, W. Zhu, X. Yuan, H. Huo, J. Gong and M. Antonietti, *Angew. Chem. Int. Ed.*, 2019, **58**, 14549-14555.
23. Z. Lu, X. Fu, J. Hou, L. Yue, J. Li, G. Ran, C. Xiao and X. Wang, *Catal. Commun.*, 2023, **177**, 106632.
24. X. Cui, R. Huang and D. Deng, *EnergyChem*, 2021, **3**, 100050.
25. N. Yusuf, F. Almomani and H. Qiblawey, *Fuel*, 2023, **345**, 128178.
26. Z. Zhang, Z. Yang, L. Liu, Y. Wang and S. Kawi, *Adv. Energy Mater.*, 2023, **13**, 2301852.
27. J. Yao, F. Cao, Y. Han, Y. Wang, L. Tan, J. Sun, G. Yang and L. Shi, *Resour. Chem. Mater.*, 2024, **3**, 62-92.
28. D. Ješić, D. Lašič Jurković, A. Pohar, L. Suhadolnik and B. Likozar, *Chem. Eng. J.*, 2021, **407**, 126799.
29. P. Ganji, R. K. Chowdari and B. Likozar, *Energy & Fuels*, 2023, **37**, 7577-7602.
30. H. Puliyalil, D. Lašič Jurković, V. D. B. C. Dasireddy and B. Likozar, *RSC Adv.*, 2018, **8**, 27481-27508.
31. L. Jiang, K. Li, W. N. Porter, H. Wang, G. Li and J. G. Chen, *J. Am. Chem. Soc.*, 2024, **146**, 2857-2875.
32. F. Liu, K. Huang, A. Zheng, F.-S. Xiao and S. Dai, *ACS Catal.*, 2018, **8**, 372-391.
33. B. H. Lipshutz, S. Ghorai and M. Cortes-Clerget, *Chem. - Eur. J.*, 2018, **24**, 6672-6695.
34. L.-H. Xie, M.-M. Xu, X.-M. Liu, M.-J. Zhao and J.-R. Li, *Adv. Sci.*, 2020, **7**, 1901758.
35. L. Liu, Z.-P. Tao, H.-R. Chi, B. Wang, S.-M. Wang and Z.-B. Han, *Dalton Trans.*, 2021, **50**, 39-58.
36. M. Qu, B. Zhang, Y. Wang, Y. Lv, J. Ge, Y. Wu, M. Yan, L. Shen and J. He, *Surf. Interface Anal.*, 2023, **55**, 279-287.
37. G. Huang, Q. Yang, Q. Xu, S. H. Yu and H. L. Jiang, *Angew. Chem. Int. Ed.*, 2016, **55**, 7379-7383.
38. W. Zong, H. Gao, Y. Ouyang, K. Chu, H. Guo, L. Zhang, W. Zhang, R. Chen, Y. Dai, F. Guo, J. Zhu, Z. Zhang, C. Ye, Y. E. Miao, J. Hofkens, F. Lai and T. Liu, *Angew. Chem. Int. Ed.*, 2023, **62**, e202218122.
39. Y. Qi, M. Yang, T.-E. Zhao, G. Tang, H. He, H. Sun, Y. Yang and C.-P. Li, *Inorg. Chem. Front.*, 2023, **10**, 2978-2986.
40. H. He, H.-K. Li, Q.-Q. Zhu, C.-P. Li, Z. Zhang and M. Du, *Appl. Catal., B*, 2022, **316**, 121673.
41. D. Kim, K. Alam, M.-K. Han, S. Surendran, J. Lim, J. Young Kim, D. Jun Moon, G. Jeong, M. Gon Kim, G. Kwon, S. Yang, T. Gon Kang, J. Kyu Kim, S. Yeop Jung, H. Cho and U. Sim, *J. Colloid Interface Sci.*, 2023, **633**, 53-59.
42. L. Niu, Z. Liu, G. Liu, M. Li, X. Zong, D. Wang, L. An, D. Qu, X. Sun, X. Wang and Z. Sun, *Nano Res.*, 2022, **15**, 3886-3893.
43. Q. Zhang, M. Zhou, G. Ren, Y. Li, Y. Li and X. Du, *Nat. Commun.*, 2020, **11**, 1731.
44. H. Wang, S. Jiang, H. Yu, K. Deng, Z. Wang, X. Li, Y. Xu and L. Wang, *J. Mater. Chem. A*, 2023, **11**
13633 -13639.
45. C. Wang, L. Liu, H. Li, L. Wang and F.-S. Xiao, *Matter*, 2023, **6**, 2697-2710.
46. J. Bai, W. Wang and J. Liu, *Chem. - Eur. J.*, 2023, **29**, e202302461.
47. W. Zhou, J. Kang, K. Cheng, S. He, J. Shi, C. Zhou, Q. Zhang, J. Chen, L. Peng, M. Chen and Y. Wang, *Angew. Chem. Int. Ed.*, 2018, **57**, 12012-12016.
48. M. Gupta, M. L. Smith and J. J. Spivey, *ACS Catal.*, 2011, **1**, 641-656.
49. J. Su, H. Zhou, S. Liu, C. Wang, W. Jiao, Y. Wang, C. Liu, Y. Ye, L. Zhang, Y. Zhao, H. Liu, D. Wang, W. Yang, Z. Xie and M. He, *Nat. Commun.*, 2019, **10**, 1297.
50. S. Lyu, Y. Wang, J. Qian, S. Liu, Z. Li, Y. Zhang, L. Wang and J. Li, *ACS Catal.*, 2021, **11**, 4278-4287.
51. F. Jiao, J. Li, X. Pan, J. Xiao, H. Li, H. Ma, M. Wei, Y. Pan, Z. Zhou, M. Li, S. Miao, J. Li, Y. Zhu, D. Xiao, T. He, J. Yang, F. Qi, Q. Fu and X. Bao, *Science*, 2016, **351**, 1065-1068.
52. Y. Xu, H. Liang, R. Li, Z. Zhang, C. Qin, D. Xu, H. Fan, B. Hou, J. Wang, X. K. Gu and M. Ding, *Angew. Chem. Int. Ed.*, 2023, **62**, e202306786.
53. E. Rytter, A. u. R. Salman, N. E. Tsakoumis, R. Myrstad, J. Yang, S. Lögdberg, A. Holmen and M. Rønning, *Catal. Today*, 2018, **299**, 20-27.
54. X. Yu, J. Zhang, X. Wang, Q. Ma, X. Gao, H. Xia, X. Lai, S. Fan and T.-S. Zhao, *Appl. Catal., B*, 2018, **232**, 420-428.
55. G. Ma, O. A. Syzgantseva, Y. Huang, D. Stoian, J. Zhang, S. Yang, W. Luo, M. Jiang, S. Li, C. Chen, M. A. Syzgantseva, S. Yan, N. Chen, L. Peng, J. Li and B. Han, *Nat. Commun.*, 2023, **14**, 501.
56. Y. Shi, Z. Li, Q. Hao, R. Li, Y. Li, L. Guo, S. Ouyang, H. Yuan and T. Zhang, *Adv. Funct. Mater.*, 2024, **34**, 2308670.
57. J. Zhao, Z. Li, P. Wang, P. Miao, R. Shi, G. I. N. Waterhouse and T. Zhang, *Nano Energy*, 2023, **110**, 108350.
58. P. Schwach, X. Pan and X. Bao, *Chem. Rev.*, 2017, **117**, 8497-8520.
59. N. Wang, K. Shen, L. Huang, X. Yu, W. Qian and W. Chu, *ACS Catal.*, 2013, **3**, 1638-1651.
60. X. Li, X. Wang, K. Roy, J. A. van Bokhoven and L. Artiglia, *ACS Catal.*, 2020, **10**, 5783-5792.
61. J. Han, D. Y. Zemlyanov and F. H. Ribeiro, *Catal. Today*, 2006, **117**, 506-513.
62. M. Cargnello, J. J. D. Jaén, J. C. H. Garrido, K. Bakhmutsky, T. Montini, J. J. C. Gámez, R. J. Gorte and P. Fornasiero, *Science*, 2012, **337**, 713-717.
63. R. Burch, F. J. Urbano and P. K. Loader, *Appl. Catal., A*, 1995, **123**, 173-184.
64. H. Wang, W. Xin, Q. Wang, X. Zheng, Z. Lu, R. Pei, P. He and X. Dong, *Catal. Commun.*, 2022, **162**, 106374.
65. W. Li, Z. Li, H. Zhang, P. Liu, Z. Xie, W. Song, B. Liu and Z. Zhao, *Proc. Natl. Acad. Sci. U. S. A.*, 2023, **120**, e2206619120.
66. W. Li, Z. Li, Z. Xie, H. Zhang, W. Song, B. Liu and Z. Zhao, *J. Catal.*, 2024, **429**, 115243.
67. S. Y. Hwang, M. Kwon, J. Hwang and E. D. Park, *Catalysts*, 2024, **14**, 280.
68. J. Sui, M.-L. Gao, B. Qian, C. Liu, Y. Pan, Z. Meng, D. Yuan and H.-L. Jiang, *Sci. Bull.*, 2023, **68**, 1886-1893.
69. H. Yang, C. Zhang, P. Gao, H. Wang, X. Li, L. Zhong, W. Wei and Y. Sun, *Catal. Sci. Technol.*, 2017, **7**, 4580-4598.
70. F. Wang, F. Chen, X. Guo, Y. He, W. Gao, S. Yasuda, G. Yang and N. Tsubaki, *Catal. Today*, 2024, **425**, 114344.
71. Y. Rodriguez Herrero and A. Ullah, *ACS Appl. Mater. Interfaces*, 2023, **15**, 14399-14414.

72. H. Li, W. Fang, L.-X. Wang, Y. Liu, L. Liu, T. Sun, C. Liao, Y. Zhu, L. Wang and F.-S. Xiao, *Innovation*, 2023, **4**, 100445.
73. H. Li, Y. Xiao, J. Xiao, K. Fan, B. Li, X. Li, L. Wang and F.-S. Xiao, *Chin. J. Catal.*, 2023, **54**, 178-187.
74. Z. Zhang, B. Chen, L. Jia, W. Liu, X. Gao, J. Gao, B. Meng, Y. Tan, Y. He, W. Tu and Y.-F. Han, *Appl. Catal., B*, 2023, **327**, 122449.
75. A. M. Appel, J. E. Bercaw, A. B. Bocarsly, H. Dobbek, D. L. DuBois, M. Dupuis, J. G. Ferry, E. Fujita, R. Hille, P. J. A. Kenis, C. A. Kerfeld, R. H. Morris, C. H. F. Peden, A. R. Portis, S. W. Ragsdale, T. B. Rauchfuss, J. N. H. Reek, L. C. Seefeldt, R. K. Thauer and G. L. Waldrop, *Chem. Rev.*, 2013, **113**, 6621-6658.
76. W. S. Dodds, L. F. Stutzman and B. J. Sollami, *Ind. Eng. Chem. Chem. Eng. Data Series*, 1956, **1**, 92-95.
77. J. Qiao, Y. Liu, F. Hong and J. Zhang, *Chem. Soc. Rev.*, 2014, **43**, 631-675.
78. J.-B. Vennekoetter, R. Sengpiel and M. Wessling, *Chem. Eng. J.*, 2019, **364**, 89-101.
79. Y. Li, F. Cui, M. B. Ross, D. Kim, Y. Sun and P. Yang, *Nano Lett.*, 2017, **17**, 1312-1317.
80. H. S. Jeon, S. Kunze, F. Scholten and B. Roldan Cuenya, *ACS Catal.*, 2018, **8**, 531-535.
81. W. Tang, A. A. Peterson, A. S. Varela, Z. P. Jovanov, L. Bech, W. J. Durand, S. Dahl, J. K. Nørskov and I. Chorkendorff, *Phys. Chem. Chem. Phys.*, 2012, **14**, 76-81.
82. P. De Luna, R. Quintero-Bermudez, C.-T. Dinh, M. B. Ross, O. S. Bushuyev, P. Todorović, T. Regier, S. O. Kelley, P. Yang and E. H. Sargent, *Nat. Catal.*, 2018, **1**, 103-110.
83. T. T. H. Hoang, S. Verma, S. Ma, T. T. Fister, J. Timoshenko, A. I. Frenkel, P. J. A. Kenis and A. A. Gewirth, *J. Am. Chem. Soc.*, 2018, **140**, 5791-5797.
84. Y. Huo, X. Peng, X. Liu, H. Li and J. Luo, *ACS Appl. Mater. Interfaces*, 2018, **10**, 12618-12625.
85. D. Higgins, C. Hahn, C. Xiang, T. F. Jaramillo and A. Z. Weber, *ACS Energy Lett.*, 2019, **4**, 317-324.
86. T. N. Huan, D. A. Dalla Corte, S. Lamaison, D. Karapinar, L. Lutz, N. Menguy, M. Foldyna, S.-H. Turren-Cruz, A. Hagfeldt, F. Bella, M. Fontecave and V. Mougel, *Proc. Natl. Acad. Sci. U. S. A.*, 2019, **116**, 9735-9740.
87. H. Mistry, A. S. Varela, C. S. Bonifacio, I. Zegkinoglou, I. Sinev, Y.-W. Choi, K. Kisslinger, E. A. Stach, J. C. Yang, P. Strasser and B. R. Cuenya, *Nat. Commun.*, 2016, **7**, 12123.
88. C. W. Li and M. W. Kanan, *J. Am. Chem. Soc.*, 2012, **134**, 7231-7234.
89. H.-Q. Liang, S. Zhao, X.-M. Hu, M. Ceccato, T. Skrydstrup and K. Daasbjerg, *ACS Catal.*, 2021, **11**, 958-966.
90. S. Mu, L. Li, R. Zhao, H. Lu, H. Dong and C. Cui, *ACS Appl. Mater. Interfaces*, 2021, **13**, 47619-47628.
91. L. Xiong, X. Fu, Y. Zhou, P. Nian, Z. Wang and Q. Yue, *ACS Catal.*, 2023, **13**, 6652-6660.
92. L. Xue, X. Wu, Y. Liu, B. Xu, X. Wang, S. Dai, P. Liu and H. Yang, *Nano Res.*, 2022, **15**, 1393-1398.
93. Y. Lin, T. Wang, L. Zhang, G. Zhang, L. Li, Q. Chang, Z. Pang, H. Gao, K. Huang, P. Zhang, Z.-J. Zhao, C. Pei and J. Gong, *Nat. Commun.*, 2023, **14**, 3575.
94. K. Lv, C. Teng, M. Shi, Y. Yuan, Y. Zhu, J. Wang, Z. Kong, X. Lu and Y. Zhu, *Adv. Funct. Mater.*, 2018, **28**, 1802339.
95. Z. Xing, X. Hu and X. Feng, *ACS Energy Lett.*, 2021, **6**, 1694-1702.
96. T. H. M. Pham, J. Zhang, M. Li, T.-H. Shen, Y. Ko, V. Tileli, W. Luo and A. Züttel, *Adv. Energy Mater.*, 2022, **12**, 2103663.
97. X. Sheng, W. Ge, H. Jiang and C. Li, *Adv. Mater.*, 2022, **34**, 2201295.
98. P. Li, J. Liu, J. Bi, Q. Zhu, T. Wu, J. Ma, F. Zhang, J. Jia and B. Han, *Green Chem.*, 2022, **24**, 1439-1444.
99. M. Wang, L. Wan and J. Luo, *Nanoscale*, 2021, **13**, 3588-3593.
100. Y. Zhang, Z. Cai, Y. Zhao, X. Wen, W. Xu, Y. Zhong, L. Bai, W. Liu, Y. Zhang, Y. Zhang, Y. Kuang and X. Sun, *Nanoscale Horizons*, 2019, **4**, 490-494.
101. R. Shi, J. Guo, X. Zhang, G. I. N. Waterhouse, Z. Han, Y. Zhao, L. Shang, C. Zhou, L. Jiang and T. Zhang, *Nat. Commun.*, 2020, **11**, 3028.
102. Z.-Z. Niu, F.-Y. Gao, X.-L. Zhang, P.-P. Yang, R. Liu, L.-P. Chi, Z.-Z. Wu, S. Qin, X. Yu and M.-R. Gao, *J. Am. Chem. Soc.*, 2021, **143**, 8011-8021.
103. M. Zhuansun, Y. Liu, R. Lu, F. Zeng, Z. Xu, Y. Wang, Y. Yang, Z. Wang, G. Zheng and Y. Wang, *Angew. Chem. Int. Ed.*, 2023, **62**, e202309875.
104. P. Yue, Q. Fu, J. Li, L. Zhang, L. Xing, Z. Kang, Q. Liao and X. Zhu, *Chem. Eng. J.*, 2021, **405**, 126975.
105. Y. Jiang, X. Zhang, D. Xu, W. Li, M. Liu and X. Qiu, *Chem. Commun.*, 2021, **57**, 6011-6014.
106. J. Shi, N. Han, B. Jin, M. Suominen, J. Lahtinen, K. Miikki, B. P. Wilson and T. Kallio, *Next Materials*, 2024, **3**, 100183.
107. S.-Q. Liu, E. Shahini, M.-R. Gao, L. Gong, P.-F. Sui, T. Tang, H. Zeng and J.-L. Luo, *ACS Nano*, 2021, **15**, 17757-17768.
108. Z. Wang, T. Li, Q. Wang, A. Guan, N. Cao, A. M. Al-Enizi, L. Zhang, L. Qian and G. Zheng, *J. Power Sources*, 2020, **476**, 228705.
109. C. Zhang, S. Yan, J. Lin, Q. Hu, J. Zhong, B. Zhang and Z. Cheng, *Processes*, 2021, **9**, 1592.
110. R. Chen, W. Tian, Y. Jia, W. Xu, F. Chen, X. Duan, Q. Xie, C. Hu, W. Liu, Y. Zhao, Y. Kuang, Y. Zhang and X. Sun, *ACS Appl. Energy Mater.*, 2019, **2**, 3991-3998.
111. Y. Li, Z. Pei, D. Luan and X. W. D. Lou, *Angew. Chem. Int. Ed.*, 2023, **62**, e202302128.
112. S. Jin, Z. Hao, K. Zhang, Z. Yan and J. Chen, *Angew. Chem. Int. Ed.*, 2021, **60**, 20627-20648.
113. K. Maeda, *Adv. Mater.*, 2019, **31**, 1808205.
114. J. L. White, M. F. Baruch, J. E. Pander, III, Y. Hu, I. C. Fortmeyer, J. E. Park, T. Zhang, K. Liao, J. Gu, Y. Yan, T. W. Shaw, E. Abelev and A. B. Bocarsly, *Chem. Rev.*, 2015, **115**, 12888-12935.
115. Z. Jiang, X. Xu, Y. Ma, H. S. Cho, D. Ding, C. Wang, J. Wu, P. Oleynikov, M. Jia, J. Cheng, Y. Zhou, O. Terasaki, T. Peng, L. Zan and H. Deng, *Nature*, 2020, **586**, 549-554.
116. P. Zhang and X. W. Lou, *Adv. Mater.*, 2019, **31**, 1900281.
117. H. Rao, L. C. Schmidt, J. Bonin and M. Robert, *Nature*, 2017, **548**, 74-77.
118. R. Kuriki, H. Matsunaga, T. Nakashima, K. Wada, A. Yamakata, O. Ishitani and K. Maeda, *J. Am. Chem. Soc.*, 2016, **138**, 5159-5170.
119. A. Call, M. Cibian, K. Yamamoto, T. Nakazono, K. Yamauchi and K. Sakai, *ACS Catal.*, 2019, **9**, 4867-4874.
120. D. Hong, T. Kawanishi, Y. Tsukakoshi, H. Kotani, T. Ishizuka and T. Kojima, *J. Am. Chem. Soc.*, 2019, **141**, 20309-20317.
121. P. Yang, Q. Zhang, Z. Yi, J. Wang and H. Yang, *J. Catal.*, 2020, **387**, 119-128.
122. B. Han, X. Ou, Z. Deng, Y. Song, C. Tian, H. Deng, Y.-J. Xu and Z. Lin, *Angew. Chem. Int. Ed.*, 2018, **57**, 16811-16815.
123. Y. Wang, S. Wang, S. L. Zhang and X. W. Lou, *Angew. Chem. Int. Ed.*, 2020, **59**, 11918-11922.
124. S. Wang, W. Yao, J. Lin, Z. Ding and X. Wang, *Angew. Chem. Int. Ed.*, 2014, **53**, 1034-1038.
125. Z. Zhu, Y. Qu, Z. Wang, F. Zhou, C. Zhao, Y. Lin, L. Li, Y. Yao and Y. Wu, *Chem. - Eur. J.*, 2020, **26**, 13601-13605.
126. Y. Liu, D. Shen, Q. Zhang, Y. Lin and F. Peng, *Appl. Catal., B*, 2021, **283**, 119630.
127. F. Li, X. Yue, L. Cheng, J. Fan and Q. Xiang, *Chem. Eng. J.*, 2023, **452**, 139463.
128. Y. Zhang, W. Qiu, Y. Liu, K. Wang, L. Zou, Y. Zhou, M. Liu, X. Qiu, J. Li and W. Li, *Chem. Commun.*, 2023, **59**, 5914-5917.
129. P. Niu, Z. Pan, S. Wang and X. Wang, *ChemSusChem*, 2021, **14**, 1302-1307.
130. F. Lin, M. Gao, Y. Wang, J. Yu, C. Gao and S. Zang, *Appl. Surf. Sci.*, 2022, **605**, 154612.
131. D. Zhao, C. Dang, Y. Xuan and Q. Zhu, *Adv. Sustainable Syst.*, 2023, **7**, 2200450.
132. E. R. Moellering, B. Muthan and C. Benning, *Science*, 2010, **330**, 226-228.
133. J. P. Dekker and E. J. Boekema, *Biochim. Biophys. Acta, Bioenerg.*, 2005, **1706**, 12-39.